IEEE Access
Multidisciplinary | Rapid Review | Open Access Journal

Received June 29, 2020, accepted July 9, 2020, date of publication July 13, 2020, date of current version July 24, 2020.

Digital Object Identifier 10.1109/ACCESS.2020.3008965

Enhanced Automated Diagnosis of Coronary Artery Disease Using Features Extracted From QT Interval Time Series and ST–T Waveform

LIANKE YAO[1], (Student Member, IEEE), CHANGCHUN LIU[1], PENG LI[2], (Member, IEEE), JIKUO WANG[1], YUANYUAN LIU[1], WANG LI[3], XINPEI WANG[1], HAN LI[1], AND HUAN ZHANG[1]

[1]School of Control Science and Engineering, Shandong University, Jinan 250061, China
[2]Division of Sleep and Circadian Disorders, Brigham and Women's Hospital, Harvard Medical School, Boston, MA 02115, USA
[3]School of Pharmacy and Bioengineering, Chongqing University of Technology, Chongqing 400054, China

Corresponding author: Changchun Liu (changchunliu@sdu.edu.cn)

This work was supported by the National Natural Science Foundation of China under Grant 61471223.

ABSTRACT There is a growing interest in automated diagnosis of coronary artery disease (CAD) with the application of machine learning (ML) methods to the body surface electrocardiograph (ECG). Although prior studies have documented associations of CAD with increased QT variability and ST–T segment abnormalities such as T-wave inversion and ST-segment elevation or depression, their efficacy in automated CAD detection has not been fully investigated. To validate their usefulness, a dataset containing related clinical characteristics and 5-min single-lead ECGs of 107 healthy controls and 93 CAD patients was first constructed. Based on this dataset, simultaneous analyses were then conducted in five scenarios, in which different ML algorithms were applied to classify the two groups with various features derived from the RR and QT interval time-series and ST–T segment waveforms. Compared with utilizing features obtained from the RR interval time-series, better classification results were achieved utilizing that obtained from the QT interval time-series. The classification results were elevated with combining utilization of features derived from both the RR and QT interval time-series. By further fusing features extracted from ST–T segment waveforms, the best performance was achieved with 96.16% accuracy, 95.75% sensitivity, and 96.40% specificity. Based the best performance, an automated CAD detection system was developed with extreme gradient boosting, an ensemble ML algorithm, and the residual neural network, namely, a deep learning method. The results of this study support the potential of information derived from the QT interval time-series and ST–T segment waveforms in ECG-based automated CAD detection.

INDEX TERMS Coronary artery disease (CAD), QT interval variability (QTV), heart rate variability (HRV), ST–T waveform, machine learning (ML), signal decomposition.

I. INTRODUCTION

Coronary artery disease (CAD), defined as an angiographic stenosis of $\geq$ 50% in at least one coronary artery, is a major type of cardiovascular disease (CVD) and the primary cause of death from CVD globally [1]–[3]. The stenosis is caused by atherogenesis, a process that narrows coronary arteries with a buildup of plaque. It can impede or even obstruct the blood flow to the heart muscle, and thus CAD patients are prone to suffer serious adverse events, e.g., arrhythmias, heart failure (HF), myocardial infarction (MI), and stroke [1]–[3]. Clinically, the surface 12-lead electrocardiogram (ECG) test is still one of the most commonly used methods of the initial screening of CAD due to its nature of non-invasiveness, low cost, and timeliness [4], [5]. Certain morphologic ECG abnormalities, including T-wave inversion, abnormal Q-wave, and ST-segment depression or elevation, have proved their clinical significance in risk stratification [6]–[8] and associations with myocardial ischemia and infarction [9]–[14]. However, these abnormalities are nonspecific symbols of CAD and can be observed in non-cardiac conditions, such as central nervous system diseases, hypothermia, and pulmonary embolism [15]. Previous studies have also reported that resting ECGs from 50 to 70% of CAD

The associate editor coordinating the review of this manuscript and approving it for publication was Filbert Juwono.

TABLE 1. An overview of existing studies on resting ECG-based automated CAD diagnosis.

Studies	Data	Features & Classifiers	Results (%)
[21]	Lead II ECGs 20 subjects (10 normal, 10 CAD)	Tunable Q wavelet transform (TQWT) based decomposition features derived from the RR interval time-series; support vector machine (SVM).	Acc = 99.72
[22]	Lead II ECGs 20 subjects (10 normal, 10 CAD)	Flexible analytic wavelet transform-based decomposition features derived from the RR interval time-series; SVM.	Acc = 100
[23]	Lead II ECGs 25 subjects (15 normal, 10 CAD)	Discrete wavelet transform (DWT) based decomposition features derived from the RR interval time-series; Gaussian mixture model.	Acc = 96.8 Sen = 100 Spe = 93.7
[20]	12-lead ECGs 47 subjects (40 normal, 7 CAD)	Higher order statistics and spectra-based bispectrum and cumulant features derived from ECGs; decision tree.	Acc = 98.99 Sen = 97.75 Spe = 99.39
[16]	Lead II ECGs 59 subjects (52 normal, 7 CAD)	Discrete cosine transform-based ECG decomposition features; K-nearest neighbors.	Acc = 98.5 Sen = 99.7 Spe = 98.5
[24]	12-lead ECGs 71 subjects (20 normal, 51 CAD)	Heart rate variability (HRV) features; multiple discriminant analysis.	Sen = 72.5 Spe = 81.8
[25]	Lead II ECGs 92 subjects (49 normal, 43 CAD)	HRV features and DWT-based ECG decomposition features; SVM.	Acc = 88.9 Sen = 84.2 Spe = 92.6
[26]	Lead II ECGs 193 subjects (94 normal, 99 CAD)	HRV features; SVM.	Acc = 90.0
[27]	Lead II ECGs 193 subjects (94 normal, 99 CAD)	HRV features and carotid arterial wall thickness features; SVM.	Sen = 90.9
This study	Lead I ECGs and clinical parameters 200 subjects (107 normal, 93 CAD)	HRV and QT interval variability features, TQWT and Hilbert-Huang transform-based decomposition features derived from both the RR and QT interval time-series, and ST–T segment waveform features derived by the ResNet-18 algorithm; extreme gradient boosting.	Acc = 96.16 Sen = 95.75 Spe = 96.40

[1] Acc: accuracy; Sen: sensitivity; Spe: specificity.

patients do not exhibit any remarkable alterations [16], [17]. Moreover, it is time-consuming and tedious for cardiologists to visually check subtle waveform abnormalities among a vast amount of ECGs. An automated detection approach can play a crucial role in addressing the above issues of ECG-based noninvasive CAD screening.

The last several decades have witnessed a growing trend towards the application of machine learning (ML) methods on ECG-based automated diagnosis of CAD which can be considered as a task of classification [18]. Some studies distinguished CAD patients from healthy individuals using publicly available datasets which consists of various labeled clinical parameters [19]. Others directly analyzed ECG or cardiac rhythm (RR interval) signals to distinguish CAD and normal sources, in which different tools derived from signal processing were applied [20]–[27]. An overview of studies using resting ECGs on automated CAD detection has been summarized in Table 1. As the table shows, the heart rate variability (HRV) analysis [24]–[27] and signal decomposition methods [21]–[23] have been utilized by most studies due to the nonstationary and nonlinear properties of physiological signals.

Meanwhile, the ventricular repolarization heterogeneity or lability as measured by beat-to-beat QT interval variability (QTV) has proved its value in risk stratification of certain CVD-related events including ventricular arrhythmia, sudden cardiac death (SCD), and cardiovascular mortality [28]–[30]. QTV quantifies the temporal fluctuation among consecutive QT intervals [31]. In comparison to normal individuals, an increase of QTV has been found in patients with HF [32]–[35] and MI [36]–[38], and in those with CAD but without MI [39]. Myocardial ischemia has also been observed to be associated with elevated QTV [40].

Additionally, as aforementioned, myocardial ischemia and infarction have been related to morphological abnormalities of the ST–T segment (also called the JT interval, which includes the ST-segment and T-wave) [9]–[14]. ST elevation is defined as one of the diagnostic criteria of acute ST elevation MI [11], and its elevation during ischemia is associated with changes in the transmembrane action potential duration and electrical cell-to-cell coupling [9]. ST depression resulting from acute MI is considered to be a reciprocal change at sites distant from the area of acute necrosis [10], [12], and the depression during ischemia is caused by current flowing in a lateral boundary between healthy and ischemic tissues [13]. T-wave alternans, referring to beat-to-beat morphological variations in the T-wave, have been observed to be increased in CAD patients and to be reduced after revascularization by percutaneous coronary intervention [14].

Despite this progress towards the clinical application of QTV and morphologic ST–T segment abnormalities, to our knowledge, their efficacy in automated CAD diagnosis with the application of ML methods has not been fully explored. Thus, the hypothesis in this study is that the utilization of information derived from ST–T segment waveforms and QT interval time-series can help enhance the performance of automated diagnosis of CAD based on single-lead resting ECGs, in comparison to the utilization of that derived from RR interval time-series. To test this hypothesis, a dataset consisting of related clinical parameters and 5-min single-lead resting ECGs of 107 healthy individuals and 93 CAD patients was first constructed. Then, simultaneous analyses were conducted in five scenarios to classify the two groups by applying different ML algorithms with various features extracted from ST–T segment waveforms and the RR and QT interval time-series. In the present study, variability and decomposition features derived from the RR and QT interval time-series were employed. Based on the best classification result from the five scenarios, a novel automated diagnostic system for CAD using related clinical characteristics and 5-min single-lead resting ECGs was further developed.

The remainder of this article is constructed as follows: Section II sequentially depicts the processes of participant recruitment, clinical characteristic and ECG acquisition, feature extraction, classification and evaluation. Section III and IV presents the results and discussion, respectively. Finally, Section V concludes this study and provides some future extensions.

II. METHODS

A. STUDY POPULATION

The study subjects included 107 healthy control subjects and 93 CAD patients who were both consecutively enrolled at Shandong Provincial Qianfoshan Hospital between November 2017 and September 2019. Healthy controls were recruited from the Physical Examination Center and were considered candidates if they had no heart disease history, were at least 40 years of age (to remove any confounding impact of age), and had normal reports on 12-lead ECG, carotid artery ultrasonography, and echocardiography (Echo) exams. Exclusion criteria for healthy subjects included advanced age ($\geq$75 years of age), mental illness, cerebrovascular diseases, thyroid dysfunction, serious hepatic or renal dysfunction, cancer, or electrolyte disturbances. CAD patients were selected from inpatients from the Department of Cardiology and who underwent the coronary angiogram. The inclusion criterion was having $\geq$ 50% lumen stenosis in at least one major coronary artery. In addition to the same exclusion criteria of the healthy controls, for the CAD patients, they were excluded if they had valve diseases, left ventricular dysfunction (ejection fraction [EF] $\leq$ 40%), or a history of HF or MI.

All subjects gave written informed consent prior to participating in this study. No attempt was made to control any medication administration. The research obtained the full approval of Clinical Ethics Committee of the aforementioned hospital, in accordance with the Declaration of Helsinki.

B. MEASUREMENTS

1) EXAMINATIONS

Information about sex, age, smoking history, weight, height, and body-mass index (BMI) was acquired from all subjects. Systolic and diastolic blood pressures (SBP and DBP) were assessed with electronic sphygmomanometers. Hypertension was defined as a baseline SBP/DBP of at least 140/90 mm Hg, or hypertension history, or under treatment with anti-hypertensive drugs [41].

Laboratory tests were performed in a central laboratory of the aforementioned hospital using an automated biochemical analyzer, with strict quality control. Following biochemical parameters were recorded, including low- and high-density lipoprotein cholesterol (LDL-C and HDL-C), glucose (GLU), total cholesterol (TC) and triglyceride (TG). Diabetes was defined as either a fasting GLU $\geq$ 7 mmol/L, or diabetes history, or on treatment with anti-diabetes medications [42]. Hyperlipidemia was defined as TG $\geq$ 1.7 mmol/L, or TC $\geq$ 5.17 mmol/L, or LDL-C $\geq$ 3.12 or HDL-C $<$ 0.78 mmol/L [43].

Echo tests were performed for all participants and carotid artery ultrasound tests were conducted only for the healthy controls using ultrasound devices by trained technicians blinded to the subjects' circumstances.

The coronary angiography was conducted only for the CAD patients according to the Judkins technique [44]. The degree of stenosis in each main coronary artery was quantified at least two vertical versions by a cardiologist blinded to the patients' circumstances.

2) VARIABILITY SIGNAL CONSTRUCTION

The ECG collection was conducted on the date of blood pressure measurement for the healthy group, and a maximum of 2 days before the coronary angiogram for the CAD patients. After a 10-min supine rest, each subject underwent a 5-min ECG recording in standard lead I configuration and sampled at a frequency of 1 kHz. Collections were completed in a quiet and temperature-controlled (25 $\pm$ 3 °C) room in the daytime using a cardiovascular function detection device.

The raw ECGs were preprocessed following the steps described in our prior work [45]. Briefly, the R-wave peak was primarily located using a detector composed of a filter bank [46], [47]. An algorithm based on line fitting was applied to detect the QRS complex onset and offset [48], and the T-wave terminus was located by seeking a marker relevant to the area under the T-wave curve [49]. Then, the delineation of above fiducial point was manually checked and ectopic beats were annotated. ECGs were eliminated if excess noise interfered with delineation or the number of ectopic beats exceeded 10% of that of the heart beats. The RR and QT interval time-series were constructed from the remaining

ECGs where abnormal intervals resulting from ectopic beats were excluded. A demonstration of fiducial point delineation is shown in Fig. 1. Examples of the RR and QT interval time-series from a healthy control and a CAD patient are displayed in Fig. 2.

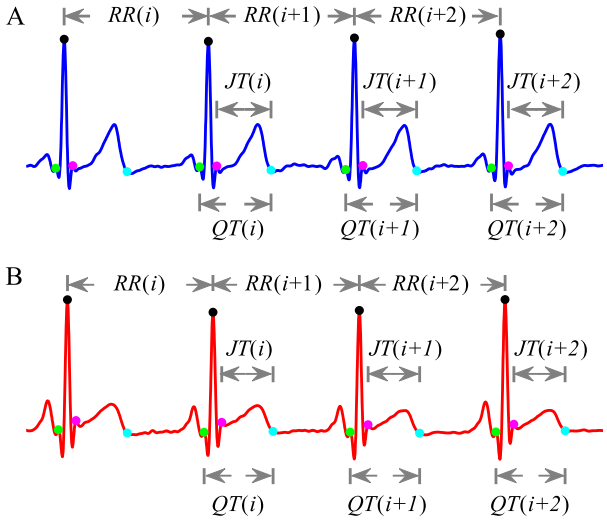

FIGURE 1. Demonstrations of fiducial point delineation for ECGs from a healthy control (blue solid line) and a CAD patient (red solid line). The detected R-wave peaks, T-wave terminus, QRS complex onsets and offsets are marked as circles with black, cyan, green, and magenta, respectively.

C. FEATURE EXTRACTION

1) VARIABILITY FEATURES

A set of 31 HRV and 19 QTV indices were computed as variability features in this study, as shown in Tables 2 and 3, respectively. Briefly, various techniques derived from signal processing in time- and frequency-domain as well as nonlinear dynamics were utilized. Given that the RR and QT interval time-series share similar properties [31], a number of indices were identical. There still existed several indicators specialized in QTV quantification, including QT variability index (QTVi), variability ratio (VR), and heart rate (HR)-corrected QT (QTc) intervals, which can all be considered as HR-normalized metrics. The purpose of their development was to minimize the influence of HR on the quantification of temporal fluctuations in beat-to-beat QT intervals.

To remove the influence of time-series length on index calculation, only the last 221 beats in each ECG were used, which accorded with the shortest length among all derived interval time-series. Prior to frequency-domain analyses, all time-series were interpolated at 4 Hz with a poly-phase filter, and then detrended using a smoothness priors algorithm [50]. Power spectral density was computed using Burg's method with an order of 16 [51]. All time-series were normalized into [0, 1] prior to nonlinear dynamics analyses.

2) DECOMPOSITION FEATURES

Considering the nonstationary and nonlinear properties of the RR and QT interval time-series, two time-frequency methods, tunable Q wavelet transform (TQWT) and Hilbert-Huang transform (HHT), were employed to acquire decomposition features.

TQWT, as an advanced wavelet transform, was proposed for analyzing discrete-time oscillatory signals, where its Q-factor (Q) and redundancy (r) could be independently and easily specified according to the signal oscillatory behavior [21]. At each level of wavelet transform, using a

TABLE 2. The heart rate variability features used in this study.

Count	Heart rate variability (HRV) feature name
31	**HRV features**
11	**Time domain features**
6	Average and standard deviation of RR interval time-series (AV_{RR} and SD_{RR}), normalized RR interval variance (RRVN), root mean square of the successive differences between adjacent RR intervals ($RMSSD_{RR}$), the standard deviation of the differences in successive RR intervals ($SDSD_{RR}$), and short-term RR interval variability (STV_{RR}) [52].
4	Numbers or percentages of pairs of successive RR intervals that differ by more than 50 or 20 ms (NN50, NN20, pNN50, and pNN20) [52].
1	HRV triangular index (HRVTi), which is computed as the ratio of integral of the density distribution to the maximum of the density distribution [52].
8	**Frequency domain features**
4	Absolute power of RR interval time-series in total (0.0033–0.4 Hz), very low (0.0033–0.04 Hz), low (0.04–0.15 Hz) and high frequency (0.15–0.4 Hz) bands (HRV_{TP}, HRV_{VLF}, HRV_{LF}, and HRV_{HF}) [52].
4	Relative VLF, LF and HF power (HRV_{VLFn}, HRV_{LFn} and HRV_{HFn}), and the LF/HF ratio for HRV ($HRV_{LF/HF}$) [52].
12	**Nonlinear dynamic features**
5	Standard deviation perpendicular the line of identity in a Poincaré plot, and its two parts corresponding to accelerations and decelerations (SD1, $SD1_{UP}$, and $SD1_{DOWN}$), and relative contributions of accelerations and decelerations (C_{UP} and C_{DOWN}) [53].
4	Porta's index (PI), Guzik's index (GI), slope index (SI), and area index (AI) [54], [55].
3	Sample entropy ($SampEn_{RR}$), fuzzy entropy ($FuzzyEn_{RR}$), and Distribution entropy ($DistEn_{RR}$) [56].

TABLE 3. The QT interval variability features used in this study.

Count	QT interval variability (QTV) feature name
19	**QTV features**
12	**Time domain features**
6	Averages and standard deviations of QT interval time-series (AV_{QT} and SD_{QT}), normalized QT interval variance (QTVN), root mean square of the successive differences between adjacent QT intervals ($RMSSD_{QT}$), short- and long-term QT interval variability (STV_{QT} and LTV_{QT}).
4	Corrected QT intervals using Bazett, Fridericia, Framingham, and Hodges formulas (QTc_{Baz}, QTc_{Frid}, QTc_{Fram}, and QTc_{Hod}).
2	QT interval variability index (QTVi), and variability ratio (VR) [31].
4	**Frequency domain features**
4	Absolute power of QT interval time-series in total, low and high frequency bands (QTV_{TP}, QTV_{LF}, and QTV_{HF}), and the LF/HF ratio for QTV ($QTV_{LF/HF}$) [31].
3	**Nonlinear domain features**
3	Sample entropy ($SampEn_{QT}$), fuzzy entropy ($FuzzyEn_{QT}$) and Distribution entropy ($DistEn_{QT}$) [56].

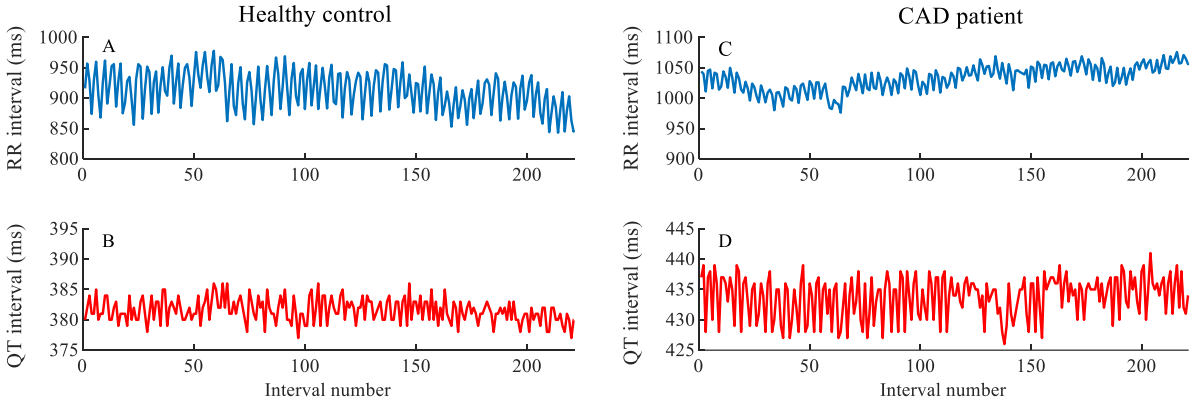

FIGURE 2. Examples of the RR and QT interval time-series displayed as blue and red solid lines, respectively. The left from a healthy control subject and the right a CAD patient.

two-channel filter bank, which consists of a low-pass filter $H_0(\omega)$ and a high-pass filter $H_1(\omega)$, the input signal with a sampling rate of f_s is decomposed into a low- and a high-pass sub-band signal with frequencies of αf_s and βf_s, respectively, where α and β are corresponding scaling parameters. The frequency responses for low- and high-pass sub-band signals acquired from the J-level can be respectively given as:

$$H_0^{(J)} := \begin{cases} \prod_{m=0}^{J-1} H_0(\omega/\alpha^m), & |\omega| \le \alpha^J \pi \\ 0, & \alpha^J \pi < |\omega| \le \pi \end{cases} \tag{1}$$

$$H_1^{(J)}(\omega) := \begin{cases} H_1(\omega/\alpha^{J-1}) \prod_{m=0}^{J-2} H_0(\omega/\alpha^m), \\ (1-\beta)\alpha^{J-1}\pi \le |\omega| \le \alpha^{J-1}\pi \\ 0, \qquad \text{for other } \omega \in [-\pi, \pi] \end{cases} \tag{2}$$

where

$$H_0(\omega) = \theta\left(\frac{\omega + (\beta-1)\pi}{\alpha+\beta-1}\right) \tag{3}$$

$$H_1(\omega) = \theta\left(\frac{\alpha\pi - \omega}{\alpha+\beta-1}\right) \tag{4}$$

and $\theta(\omega)$ is the frequency response of the Daubechies filter and can be given as:

$$\theta(\omega) = 0.5(1+\cos(\omega))\sqrt{2-\cos(\omega)}, \qquad |\omega| \le \pi \tag{5}$$

The Daubechies filter was chosen to ensure the good time-frequency localization properties of the synthesis functions of the constructed wavelet transform [57], [58]. The values of r and Q can be determined based on α and β as follows:

$$r = \beta/(1-\alpha), \quad Q = (2-\beta)/\beta \tag{6}$$

All resulting sub-band signals can be given in the manner of a cell array C:

$$C = \{w_1, w_2, w_3, \ldots, w_J, w_{J+1}\} \tag{7}$$

where ω_{J+1} is the sub-band signal of the lowest frequency and ω_1 to ω_J are the sub-band signals corresponding to the high frequency. In this study, we set $Q = 2$, $r = 4$, and $J = 3$ as recommended by [21]. Hence, a total of 4×221 wavelet features (coefficients) were acquired from the RR and QT interval time-series, respectively.

HHT is a two-step adaptive signal processing technique consisting of the empirical mode decomposition (EMD) and the Hilbert transform (HT). HHT can adaptively decompose signals according to their properties, which means it can provide more meaningful representations of nonstationary and nonlinear processes [59]. The EMD as the first step decomposes the input signal into various intrinsic mode functions (IMFs) following an iterative procedure termed the sifting process [59]. The HT is employed to acquire the Hilbert spectrum of the input signal specified by IMFs. In this work, the instantaneous frequency (IF) and instantaneous energy (IE) of each IMF were calculated as decomposition features. The EMD algorithm is summarized as follows:

1) Determine the local maxima and local minima of the input signal $x(t)$.
2) Using the cubic spline interpolation technique, acquire the envelope $E_{max}(t)$ by connecting all maxima and the $E_{min}(t)$ by connecting all minima.
3) Compute the average of $E_{max}(t)$ and $E_{min}(t)$ as:

$$m(t) = [E_{\max}(t) - E_{\min}(t)]/2 \tag{8}$$

4) Extract $k(t)$ from $x(t)$ as:

$$k(t) = x(t) - m(t) \tag{9}$$

5) Check whether $k(t)$ satisfies the following two criteria: (a) the number of extrema (maxima and minima) and that of zero-crossings in the input signal should be either equal to or differ at the largest by one; (b) at any point, the average value of two envelopes, one formed with local minima and the other formed connecting local maxima, should both be zero.
6) Repeat steps 1) to 5) until $k(t)$ satisfies the above two conditions.

Once the IMFs were outputted, for each IMF, its analytic signal, $z_i(t)$, was computed using the HT:

$$z_i(t) = c_i(t) + jH\{c_i(t)\} \tag{10}$$

where $H\{x_i(t)\}$ is the HT of i-th IMF $c_i(t)$. The $z_i(t)$ can also be expressed as:

$$z_i(t) = a_i(t)e^{j\theta_i(t)} \tag{11}$$

where $a_i(t)$ is the instantaneous amplitude and $\theta_i(t)$ is the instantaneous phase. The IE can be computed as:

$$IE_i(t) = |a_i(t)|^2 \tag{12}$$

while the IF is defined as:

$$IF_i(t) = d\theta_i(t)/dt \tag{13}$$

In the present study, the RR and QT interval time-series were decomposed into 3 levels of IMFs. Therefore, a total of 3 × 221 IE and 3 × 221 IF features (coefficients) were obtained from RR and QT interval time-series, respectively.

3) DIMENSIONALITY REDUCTION

Statistical based feature selection methods and the principal component analysis (PCA) were performed successively to reduce the dimensionality of decomposition features.

Statistical-based feature selection was conducted using an independent sample T test when the distribution normality of the untransformed feature data (or the Box-Cox transformed ones) was verified by the Shapiro–Wilk test; otherwise, the Mann–Whitney U test was performed. Homogeneity of variances was checked with the Levene's test. Features with P-value $< 10^{-3}$ were considered as discriminative ones.

The PCA was further applied to reduce dimensionality by projecting high-dimensional data onto an equal or lower amount of orthogonal variables termed principal components (PCs). Let $\boldsymbol{X}$ be an n-by-d input matrix consisting of n data points in each dimension d, the PCA algorithm could be briefly summarized as:

1) Normalize the scale of the input matrix by subtracting the respective mean in the respective column.
2) Calculate the covariance matrix of the normalized matrix.
3) Using the singular value decomposition method, obtain the eigenvalues and eigenvectors of the covariance matrix, and then sort the eigenvectors in a descending order of their eigenvalues.
4) To acquire the PCs, project the original matrix into the directions of the ordered eigenvectors by taking the dot product.
5) Choose several PCs depending on the containment of a given percentage of variability.

In this study, the PCs that explained 95% of the total variances were selected. Finally, regarding the RR and QT interval time-series, 1 and 65 PCs were obtained from their TQWT features, 13 and 50 PCs from the IE coefficients, and 1 and 3 PCs from the IF coefficients, respectively.

D. CLASSIFICATION AND EVALUATION

Statistical analyses were performed with the procedures of statistical-based feature selection to study the differences in clinical characteristics, HRV and QTV indices between the healthy controls and CAD patients. A significant difference was defined as a P-value < 0.05.

To assess the efficacy of features derived from the QT interval time-series and the ST–T segment waveforms, the classification of healthy controls and CAD patients was performed in five scenarios:

Scenario I: classification by three different ML classifiers, using the combination of clinical parameters, HRV features, and decomposition features derived from RR interval time-series. The three ML classifiers were Gaussian naive Bayes (GNB) [60], support vector machine (SVM) [61], and extreme gradient boosting (XGBoost) [62].

Scenario II: classification by the same three ML classifiers, using the combination of clinical parameters, QTV features, and decomposition features derived from QT interval time-series.

Scenario III: classification by the same three ML models, using the combination of clinical characteristics, HRV and QTV features, and decomposition features extracted from both the RR and QT interval time-series.

Scenario IV: classification by the residual neural network with 18-layer deep (ResNet-18) [63] using ST–T segment waveforms.

Scenario V: classification by the ML classifier exhibiting the best classification results among the above three models, with the combining utilization of clinical parameters, HRV and QTV features, decomposition features extracted from both the RR and QT interval time-series, and morphologic ST–T segment features derived by the ResNet-18 algorithm.

To evaluate classification performance in each scenario, five-fold cross-validation was conducted, in which four out of five parts of the dataset were utilized as a training set and the rest as a test set. During the cross-validation process, the same dataset split was adopted in each scenario. In scenarios IV and V, ST–T segments were derived from the heart beats used for constructing the RR and QT interval time-series, and prior to analyses interpolation/decimation was applied to adjust all segments to have the same length. Each feature was scaled by mapping its minimum and maximum values into [0, 1] prior to classification. Parameter setup for each used ML method is presented in Supplementary Table 1. Final results were reported as the average of accuracy (Acc), sensitivity (Sen), and specificity (Spe) via the five-fold cross validation. The raw ECG preprocessing, variability and decomposition feature extraction were implemented using MATLAB 2018a, and classification experiments were conducted in Python 3.7. All experiments were performed on a PC with Intel Core i7 CPU, 16 GB RAM, NVDIA GeForce GTX 1080Ti GPU, and Linux Ubuntu 14.04.

III. RESULTS

A. CHARACTERISTICS OF THE SUBJECTS

Clinical characteristics of all of the subjects are displayed in Table 4, and the comparative results between the CAD

TABLE 4. Clinical characteristics of the subjects.

Clinical characteristics	Ranges
Age (years)	41–74
Sex	Male, female
Weight (kg)	45–102.2
Height (cm)	148.5-190
Body-mass index (kg/m^2)	17.3–33.2
Systolic blood pressure (mmHg)	90–193
Diastolic blood pressure (mmHg)	47–114
Smoking history	Yes, no
Diabetes mellitus	Yes, no
Hypertension	Yes, no
Hyperlipidemia	Yes, no
Glucose (mmol/L)	3.96–13.60
Triglycerides (mmol/L)	0.34–11.11
Total cholesterol (mmol/L)	2.36–7.82
HDL-C (mmol/L)	1.05–5.68
LDL3-C (mmol/L)	0.40–4.59

[1] HDL-C and LDL-C: high- and low-density lipoprotein cholesterol.

patients and healthy controls are shown in Supplementary Table 2. The CAD patients were taller ($P < 0.05$) and had higher SBP ($P < 10^{-3}$) compared with the healthy controls. Meanwhile, the CAD patients had a remarkably increased prevalence of a smoking history ($P < 0.01$), hypertension ($P < 10^{-10}$), and diabetes ($P < 10^{-6}$) than the healthy control group. The concentration of TC was significantly lower in the CAD patients than in the healthy controls ($P < 10^{-4}$). In contrast, the levels of LDL-C and GLU were markedly higher in CAD patients than in healthy control subjects ($P < 10^{-7}$ and 0.05, respectively).

B. VARIABILITY FEATURES

Comparative results of the studied HRV and QTV markers that showed statistically significant differences between the healthy controls and CAD patients are exhibited in Tables 5 and 6, respectively. As displayed in Table 5, significant differences were expressed by 17 of 31 HRV features, and nearly all of these 17 HRV indices were markedly lower in the CAD patients than in the healthy controls, except the relatively high frequency power of HRV (HRV_{HFn}). As displayed in Table 6, significant differences were exhibited by 17 of 19 QTV features, and all of these 17 QTV indices were strikingly higher in the CAD patients compared with the healthy controls.

C. DECOMPOSITION FEATURES

The TQWT-based decomposition features derived from the example RR and QT interval time-series are shown in Figs. 3 and 4, respectively. On the first level, the features computed from both the RR and QT interval time-series of the example CAD patient were higher than that derived from the healthy control. Visually, on the other three levels, there were more fluctuations among the coefficients obtained from the CAD patient than in that extracted from the healthy control.

The IE coefficients derived from the example RR and QT interval time-series are shown in Figs. 5 and 6, respectively.

TABLE 5. Comparative results of studied HRV indices between healthy controls and CAD patients.

Variables	Healthy controls (N = 107)	CAD patients (N = 93)	P
SD_{RR} (ms)	31.79 ± 12.13	23.39 ± 10.67	$<10^{-7}$
$RMSSD_{RR}$ (ms)	22.41 ± 12.14	17.49 ± 9.57	<0.01
$SDSD_{RR}$ (ms)	22.46 ± 12.17	17.53 ± 9.59	$<10^{-7}$
STV_{RR} (ms)	12.76 ± 7.19	10.04 ± 5.65	<0.01
RRVN	1.30 ± 0.88	0.75 ± 0.71	$<10^{-8}$
NN50	6.12 ± 10.69	3.12±9.20	$<10^{-3}$
pNN50 (%)	2.76 ± 4.82	1.40 ± 4.14	$<10^{-3}$
NN20	35.40 ± 26.36	25.34 ± 22.42	<0.01
pNN20 (%)	15.95 ± 11.87	11.42 ± 10.10	<0.01
HRVTi	8.08 ± 2.43	6.28 ± 2.26	$<10^{-7}$
HRV_{LF} (ms^2)	3.56 ± 0.98	2.74 ± 1.01	$<10^{-7}$
HRV_{HF} (ms^2)	8.14 ± 1.25	7.76 ± 1.21	<0.05
$HRV_{LF/HF}$ (%)	43.38 ± 9.12	34.65 ± 10.90	$<10^{-9}$
HRV_{VLFn} (%)	11.60 ± 5.84	5.92 ± 11.14	$<10^{-6}$
HRV_{LFn} (%)	26.28 ± 2.94	23.12 ± 4.62	$<10^{-7}$
HRV_{HFn} (%)	62.12 ± 7.96	70.92 ± 15.27	$<10^{-7}$
$DistEn_{RR}$	0.80 ± 0.07	0.74 ± 0.07	$<10^{-7}$

[1] Values are mean ± standard deviation (SD); only the studied HRV indices showing statistically significant differences are presented.

TABLE 6. Comparative results of studied QTV indices between healthy controls and CAD patients.

Variables	Healthy controls (N = 107)	CAD patients (N = 93)	P
QTc_{Baz} (ms$^{1/2}$)	403.92 ± 21.45	420.79 ± 22.99	$<10^{-6}$
QTc_{Frid} (ms$^{2/3}$)	397.52 ± 19.04	414.41 ± 20.21	$<10^{-8}$
QTc_{Fram} (ms)	386.12 ± 27.87	402.80 ± 25.04	$<10^{-4}$
QTc_{Hod} (ms)	385.72 ± 27.85	402.40 ± 25.03	$<10^{-4}$
AV_{QT} (ms)	385.82 ± 27.85	402.41 ± 1.28	$<10^{-4}$
SD_{QT} (ms)	2.85 ± 0.98	3.41 ± 1.28	<0.01
QTVN	6.03 ± 4.86	8.23 ± 7.43	<0.05
$RMSSD_{QT}$ (ms)	2.53 ± 0.74	4.28 ± 1.92	$<10^{-13}$
STV_{QT} (ms)	1.37 ± 0.41	2.33 ± 1.07	$<10^{-13}$
LTV_{QT} (ms)	543.18 ± 39.21	566.67 ± 35.24	$<10^{-4}$
QTVi	-1.33 ± 0.31	-0.93 ± 0.46	$<10^{-10}$
VR	0.14 ± 0.09	0.32 ± 0.30	$<10^{-11}$
QTV_{TP} ($_{P}$ms^2)	4.44 ± 0.54	5.37 ± 0.83	$<10^{-15}$
QTV_{LF} (ms^2)	3.19 ± 0.64	4.00 ± 0.85	$<10^{-11}$
QTV_{HF} (ms^2)	4.07 ± 0.54	5.06 ± 0.85	$<10^{-16}$
$FuzzyEn_{QT}$	1.35 ± 0.23	1.52 ± 0.16	$<10^{-7}$
$DistEn_{QT}$	0.40 ± 0.05	0.42 ± 0.06	<0.01

[1] Values are mean ± standard deviation (SD); only the studied QTV indices showing statistically significant differences are presented.

As displayed in Fig. 5, on the IMF1 and IMF2 levels, the IE coefficients of the CAD patient exhibited more upward spikes than that of the healthy individual. However, there were no visually significant changes between the two subjects on the IMF3 level. Regarding to the results of the QT interval time-series (Fig. 6), on all three levels, IE coefficients of the CAD patient are strikingly higher compared with that of the healthy control. Detailed coefficients of the healthy control are shown in Fig. 10.

The IF coefficients derived from the example RR and QT interval time-series on the basis of HHT are shown in Figs. 7 and 8, respectively. On the IMF1 and IMF2 levels, visually, the IF features derived from both the RR and QT interval time-series of the CAD patient exhibited more downward spikes than that of the healthy control. However, on the

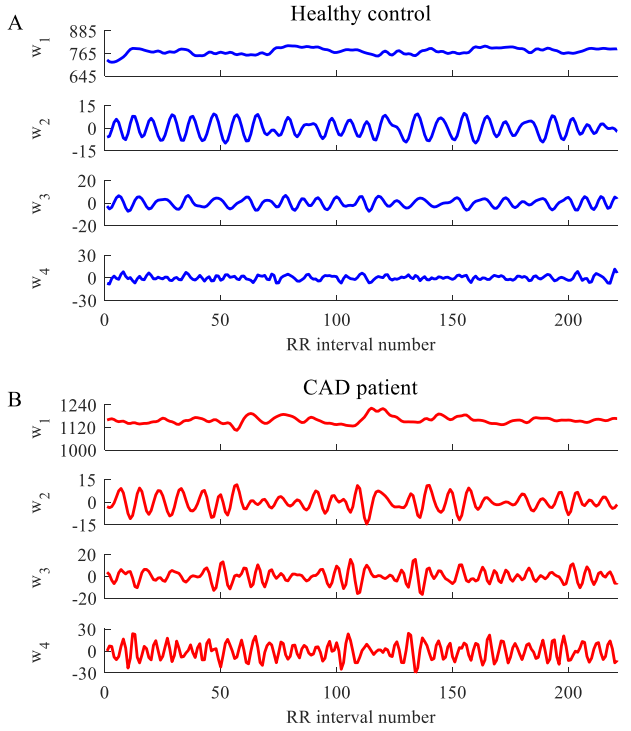

FIGURE 3. Tunable Q wavelet transform-based decomposition features of the example RR interval time-series displayed in Figure 2. Shown upper from a healthy control subject and bottom from a CAD patient.

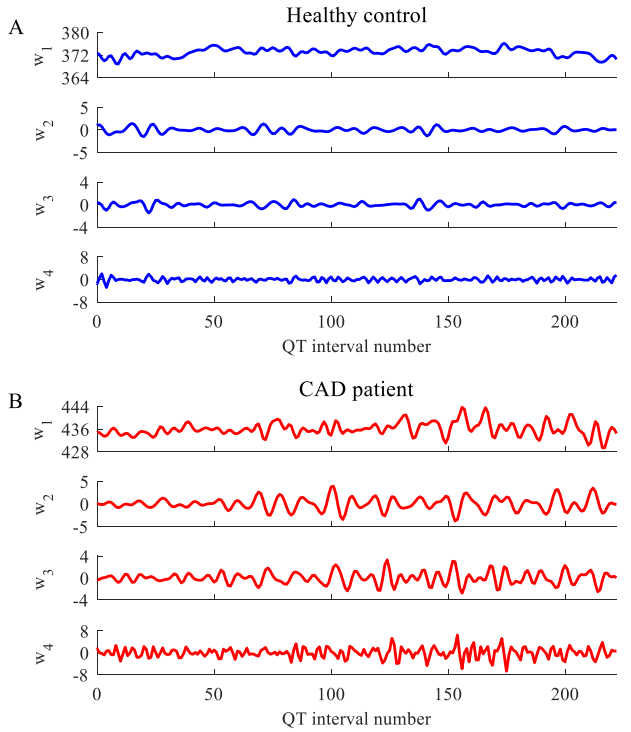

FIGURE 4. Tunable Q wavelet transform-based decomposition features of the example QT interval time-series displayed in Figure 2. Shown upper from a healthy subject and bottom a CAD patient.

IMF3 level, no remarkable differences between the example two subjects were observed for the IF features of the RR and QT interval time-series.

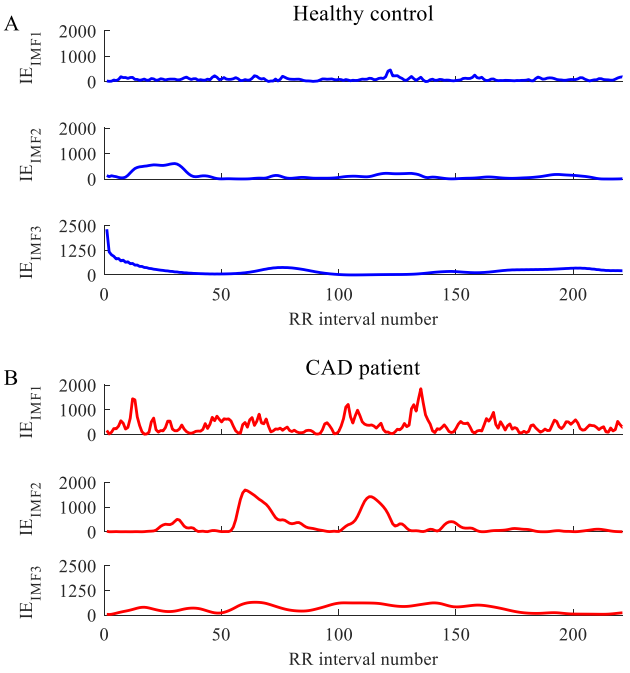

FIGURE 5. Hilbert-Huang transform-based instantaneous energy decomposition features of the example RR interval time-series shown in Figure 2. Shown upper from a healthy control subject and bottom a CAD patient.

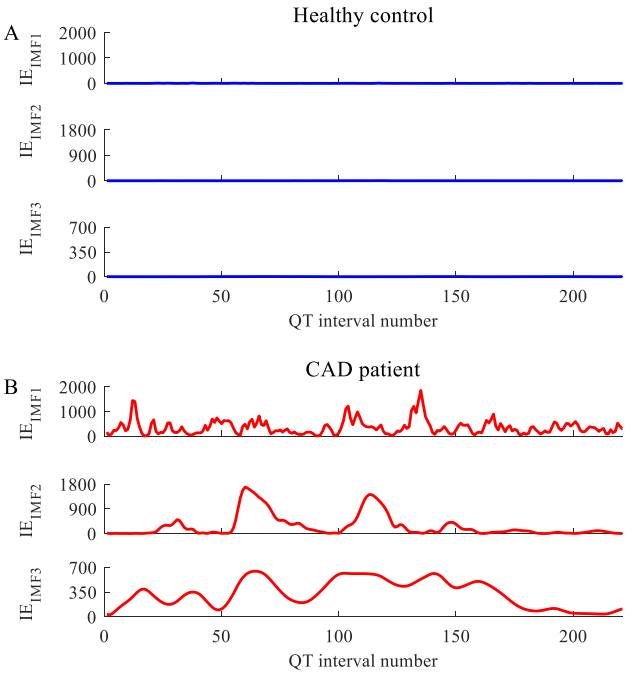

FIGURE 6. Hilbert-Huang transform-based instantaneous energy decomposition features of the example QT interval time-series shown in Figure 2. Shown upper from a healthy control subject and bottom a CAD patient.

D. CLASSIFICATION

Table 7 shows the classification results in five different scenarios. In general, the classification performances of all three

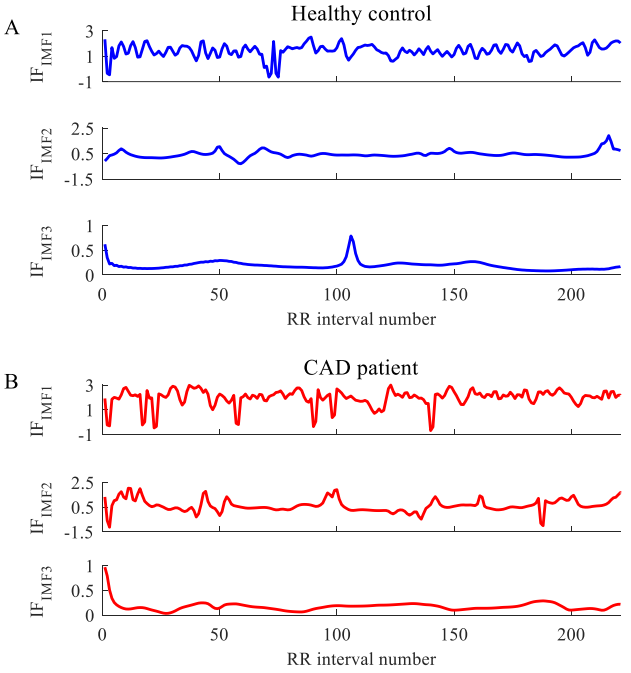

FIGURE 7. Hilbert-Huang transform-based instantaneous frequency decomposition features of the example RR interval time-series shown in Figure 2. Shown upper from a healthy control subject and bottom a CAD patient.

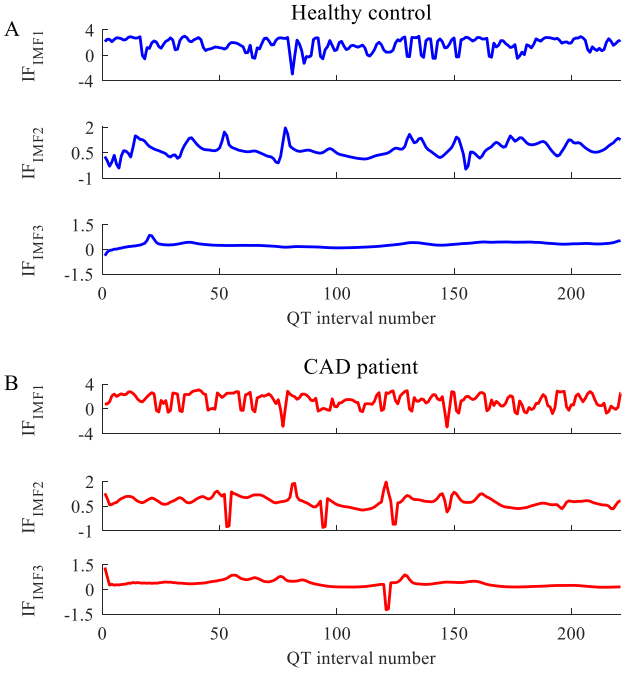

FIGURE 8. Hilbert-Huang transform-based instantaneous frequency decomposition features of the example QT interval time-series shown in Figure 2. Shown upper from a healthy control subject and bottom a CAD patient.

applied ML methods improved from scenario I to III. A comparison between scenarios I and II indicated that the utilization of features derived from QT interval time-series can achieve better classification results than the utilization of that derived from the RR interval time-series. Likewise, the comparisons among scenarios I, II and III suggested that, for one thing, the QT interval time-series can provide additionally helpful information as compared with the RR interval time-series; for another, the combination of the features acquired from both the RR and QT interval time-series can achieve better classification performances than the utilization of that derived from either the RR or QT interval time-series. Admittedly, a direct analysis of ST–T segment waveforms with ResNet-18 (scenario IV) did not achieve comparable results with other four scenarios, but a comparison between the scenarios III and V suggested the benefit of the utilization of features derived from ST–T segment waveforms. A possible interpretation may be that, although the information provided by the ST–T segment waveform from single-lead ECGs was limited, it can still potentially be helpful for automated CAD detection. Based on the classification results of the scenario V, a novel ECG-based automated system for detecting CAD was further summarized in Fig. 9.

IV. DISCUSSION

To explore the efficacy of utilizing QT interval time-series and ST–T segment waveforms for automated diagnosis of CAD with ML methods, this study primarily constructed a dataset consisting of related clinical parameters and 5-min single-lead resting ECGs of 107 healthy controls and 93 CAD patients. Based on this dataset, simultaneous analyses were then conducted in five scenarios in which various features derived from ST–T segment waveforms and the RR and QT interval time-series were employed. The results showed that the utilization of decomposition and variability features derived from the QT interval time-series performed better than the application of that derived from the RR interval time-series. The results also indicated that, among the five scenarios, the best classification performance was achieved when using a combination of decomposition and variability features derived from the RR and QT interval time-series, ST–T segment waveform features extracted by the ResNet-18 algorithm, and relevant clinical parameters, with 96.16% accuracy, 95.75% sensitivity, and 96.40% specificity.

The most important finding of the present study was that, in automated CAD diagnosis by applying ML methods with single-lead resting ECGs, the utilization of features derived from the QT interval time-series can enhance classification performance than the application of that derived from the RR interval time-series. QTV in body surface ECG is understood as a measure of ventricular repolarization heterogeneity or lability [31]. Elevated QTV in CAD patients compared with healthy subjects has been attributed to a more heterogeneous final phase of ventricular repolarization due to the reduced coronary blood flow [39]. Previous research has reported significant differences between ischemic and non-ischemic episodes in QTVi and normalized QTV marker, but not in normalized HRV index [40]. Additionally, ML methods have been applied to characterize side effects of anti-arrhythmic

TABLE 7. Results of classification in five different scenarios.

Features	Classifiers	Accuracy (%)	Sensitivity (%)	Specificity (%)
Heart rate variability (HRV) indices, decomposition features derived from RR interval time-series, and clinical parameters (scenario I)	Gaussian naive Bayes	72.09 ± 4.71	72.19 ± 5.42	71.58 ± 8.79
	Support vector machine	74.97 ± 5.53	75.61 ± 5.19	75.37 ± 8.68
	XGBoost	72.46 ± 3.78	72.86 ± 4.64	72.85 ± 7.74
QT interval variability (QTV) indices, decomposition features derived from QT interval time-series, and clinical parameters (scenario II)	Gaussian naive Bayes	81.52 ± 4.37	81.05 ± 4.47	83.16 ± 6.54
	Support vector machine	81.44 ± 1.60	79.98 ± 6.93	82.56 ± 5.39
	XGBoost	91.54 ± 3.89	92.63 ± 6.53	90.69 ± 3.78
HRV and QTV indices, decomposition features derived from both RR and QT interval time-series, and clinical parameters (scenario III)	Gaussian naive Bayes	79.18 ± 4.33	78.88 ± 6.86	79.61 ± 4.52
	Support vector machine	87.05 ± 2.88	88.78 ± 5.84	85.31 ± 4.01
	XGBoost	92.54 ± 1.46	92.46 ± 2.62	92.57 ± 2.51
ST–T segment waveforms (scenario IV)	ResNet-18	78.46 ± 5.64	72.89 ± 4.53	83.37 ± 2.89
ST–T segment waveforms, QTV and HRV indices, decomposition features derived from RR and QT interval time-series, and clinical characteristics (scenario V)	ResNet-18 and XGBoost	96.16 ± 2.97	95.75 ± 2.51	96.40 ± 4.89

[1] Values are mean ± standard deviation (SD); XGBoost: extreme gradient boosting; ResNet-18: residual neural network with 18-layer deep.

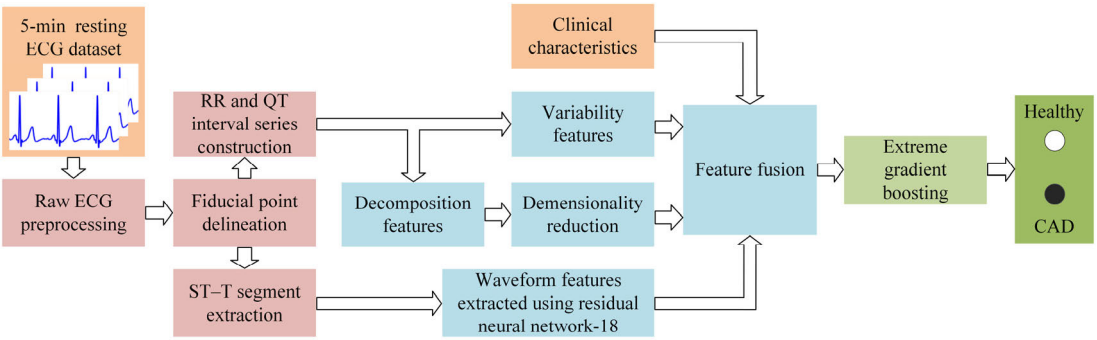

FIGURE 9. block diagram of the system stemmed from the scenario V for ECG-based automated diagnosis of coronary artery disease (CAD).

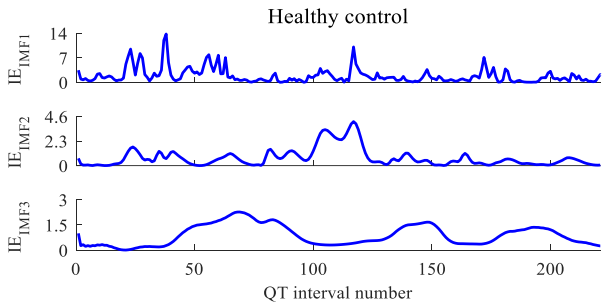

FIGURE 10. Hilbert-Huang transform-based instantaneous energy (IE) decomposition features of the example QT interval time-series of the healthy control displayed in Figure 2.

drugs on the QT interval, and an excellent agreement has been observed between QT interval changes predicted by ML models and that observed in a randomized clinical trial [64]. An ML process by applying the GNB model has been developed to distinguish children with and without long QT syndrome (LQTS) [65]. An ion channel-specific ML method has also been proposed to predict the potential functional influence of rare KCNQ1 genetic variants, one of the three major LQTS-susceptibility genes [66]. With above progress in applying ML algorithms with the QT interval analysis, enhanced classification results by utilizing features from the QT interval time-series and ST–T segment waveform in this study, while preliminary, has important implications for the clinical application of the QTV analysis and the development of more comprehensible automated diagnosis of CAD for cardiologists.

In addition, as a major physiological source of QTV [31], HRV that reflects the autonomous nervous system (ANS) activity also influences QTV at the cellular, tissue, and organ levels [67]. QT intervals are affected by the preceding RR intervals through the cellular dependency of APD, which mainly consists of rapid and slow adaptation processes [67]. Decoupling between the RR and QT interval has been found during myocardial ischemia episodes [31]. In experimentally induced HF animals, QTV elevation has also been observed when the sympathetic nerve was activated [31]. Though the QT–RR relation is important for the QTV analysis, clinical value of the dynamic response of the QT interval to the RR interval in the CAD patient remains largely unknown [31]. Further research should be undertaken to explore the efficacy of utilizing information about the QT–RR relation with ML models in automatic detection of CAD.

Another important finding was that a comparison between the classification results in scenario III and IV (Table 7)

TABLE 8. Model parameter setup.

Models	Parameters
Gaussian Naive Bayes	Non-specified prior probabilities, portion of the largest variance = 1×10^{-9}
Support vector machine	Regularization parameter = 100, kernel = radial basis function, tolerance for stopping criterion = 1×10^{-3}, kernel coefficient = the reciprocal of the number of features
Extreme gradient boosting	Booster = tree-based models, learning rate = 0.05, minimum loss reduction = 0, maximum depth of a tree = 5, minimum sum of instance weight = 7, maximum delta step = 0, subsample ratio of the training instances = 0.8, subsample ratio of columns = 0.6, random number seed = 3, L2 regularization term on weights = 1, L1 regularization term on weights = 0, the initial prediction score = 0.5, the number of boosting rounds = 7, the tree construction algorithm = use heuristic to choose the fastest method, objective = logistic regression for binary classification, evaluation metrics for validation data = area under the curve, the method used to sample the training instances = uniform
Residual neural network with 18-layer deep	Learning rate = 1×10^{-3}, batch size = 500, optimizer = Adam [69], loss function = cross entropy, epoch = 10, weight decay = 5×10^{-4}

TABLE 9. Comparative results of clinical characteristics between included healthy controls and CAD patients.

Clinical characteristics	Healthy controls (N = 107)	CAD patients (N = 93)	*P*
Age (years)	61.00 (55.00–66.00)	63.00 (56.00–69.00)	0.11
Sex	67 (62.62)	56 (60.22)	0.77
Weight (kg)	72.22 ± 11.18	71.34 ± 10.30	0.57
Height (cm)	168.50 (164.00–176.00)	168.00 (159.50–172.00)	<0.05
Body-mass index (kg/m^2)	25.04 ± 2.93	25.68 ± 3.05	0.17
Systolic blood pressure (mmHg)	123.00 (115.00–138.00)	131.00 (121.50–144.00)	$<10^{-3}$
Diastolic blood pressure (mmHg)	78.77 ± 12.66	78.48 ± 12.57	0.88
Smoking history	22 (20.56)	37 (39.78)	<0.01
Hyperlipidemia (N; %)	17 (20.56)	19 (20.43)	0.46
Hypertension (N; %)	18 (16.82)	57 (61.29)	$<10^{-10}$
Diabetes mellitus (N; %)	5 (4.67)	30 (32.26)	$<10^{-6}$
Glucose (mmol/L)	5.13 (4.81–5.56)	5.45 (4.88–6.60)	<0.05
Triglycerides (mmol/L)	1.16 (0.88–1.75)	1.32 (1.05–1.94)	0.06
Total cholesterol (mmol/L)	5.05 ± 0.99	4.44 ± 1.03	$<10^{-4}$
HDL-C (mmol/L)	2.84 ± 0.82	2.64 ± 0.86	0.09
LDL-C (mmol/L)	1.31 (1.08–1.55)	1.07 (0.91–1.27)	$<10^{-7}$

[1] Values are mean ± standard deviation (SD), frequencies (percentages), or median (interquartile range [IQR]), as appropriate; HDL-C and LDL-C: high- and low-density lipoprotein cholesterol.

suggested the benefit of utilizing ST–T segment waveforms in ECG-based automated CAD detection. Clinically, when ST–T abnormalities are manually detected, the cardiologists need to take into account many other sources of information (such as patient descriptions, anamnesis, and symptoms) and all of the other differential diagnoses [68]. Since myocardial ischemia-related ST–T abnormalities can also be found in other cardiac and noncardiac conditions, a diagnosis based on only ST–T abnormalities might result in high sensitivity and poor specificity [68]. There are several studies that have used decomposition features derived from ECGs [16], [25], as shown in Table 1. The findings from the present study suggested that a special focus on the ECG segment relevant to myocardial ischemia may facilitate ECG-based automated diagnosis of CAD. Despite this promising finding, further work is required to develop a full picture of the advantages of applying ST–T segments with ML algorithms.

Our study has several limitations. A dataset with a larger subject population would certainly improve the results. Since subjects older than 75 years old were excluded in the present study, an extension on subjects with advanced ages would also enhance the implications of this study. The investigation was conducted on CAD patients without MI, in comparison to healthy control subjects; thus, our findings might not be applicable to MI patients. The findings were only tested on the constructed database. Validation on other datasets would definitely further confirm the usefulness of ST–T segment waveforms and QT intervals in ECG-based automated CAD detection. The possibility of medication effects on the results cannot be excluded. The QT and RR interval time-series derived from only 5-min single-lead ECGs were used in this work. The utilization of 12-lead or long-term ECGs would extend the clinical applications of our findings. Considering that the T-wave end determination is still a challenge, the QT interval measurement error might result in excess noises and further impact the results.

V. CONCLUSION

To explore the efficacy of the information derived from QT interval time-series and ST–T segment waveforms in ECG-based automated CAD detection, this study first constructed a dataset which consists of related clinical characteristics and 5-min single-lead resting ECGs of 107 healthy controls and 93 CAD patients. Based on this dataset, simultaneous analyses were then conducted in five scenarios, in which different ML models were applied to classify the two

groups using various features derived from the RR and QT interval time-series and ST–T segment waveforms. Decomposition and variability features were extracted from the RR and QT interval time-series, and a deep learning model, ResNet-18, was applied to extract ST–T segment waveform features. The classification results showed that better classification results were observed utilizing features extracted from the QT interval time-series compared with utilizing those derived from the RR interval time-series. The best classification results were achieved using a combination of above features derived from the RR and QT interval time-series and the ST–T segment waveforms, with 96.16% accuracy, 95.75% sensitivity, and 96.40% specificity. Based on the best results, a novel automated diagnostic system for CAD was developed. Our study results suggest that the features extracted from QT interval time-series and ST–T segment waveforms have potential in automated detection of CAD based on single-lead resting ECGs and ML methods.

APPENDIX

See Tables 8 and 9.

ACKNOWLEDGMENT

The authors would like to extend our gratitude to Y. Li and Y. Jiao of the Institute of Biomedical Engineering at Shandong University, as well as all the nurses of the No. 45 inpatient area at Shandong Provincial Qianfoshan Hospital for their assistance with the data acquisition.

REFERENCES

[1] A. Timmis, N. Townsend, C. P. Gale, and A. Torbica, "European society of cardiology: Cardiovascular disease statistics 2019," *Eur. Heart J.*, vol. 41, no. 1, pp. 12–85, Jan. 2020, doi: 10.1093/eurheartj/ehz859.

[2] S. S. Virani, A. Alonso, and E. J. Benjamin, "Heart disease and stroke Statistics—2020 update: A report from the American heart association," *Circulation*, vol. 141, no. 9, pp. 139–596, Mar. 2020, doi: 10.1161/CIR.0000000000000757.

[3] L. Y. Ma, W. W. Chen, R. L. Gao, L. S. Liu, and M. L. Zhu, "China cardiovascular diseases report 2018: An updated summary," *J. Geriatric Cardiol.*, vol. 17, no. 1, pp. 1–8, Jan. 2020, doi: 10.11909/j.issn.1671-5411.2020.01.001.

[4] R. Auer, "Association of major and minor ECG abnormalities with coronary heart disease events," *JAMA*, vol. 307, no. 14, pp. 1497–1505, Apr. 2012, doi: 10.1001/jama.2012.434.

[5] B. J. Maron, "Assessment of the 12-lead ECG as a screening test for detection of cardiovascular disease in healthy general populations of young people (12-25 years of age): A scientific statement from the American heart association and the American college of cardiology," *Circulatation*, vol. 130, no. 15, pp. 1303–1334, Oct. 2014, doi: 10.1161/CIR.0000000000000025.

[6] D. E. Haines, D. S. Raabe, W. D. Gundel, and F. J. Wackers, "Anatomic and prognostic significance of new T-wave inversion in unstable angina," *Amer. J. Cardiol.*, vol. 52, no. 1, pp. 14–18, Jul. 1983, doi: 10.1016/0002-9149(83)90061-9.

[7] N. S. Tan, S. G. Goodman, R. T. Yan, B. Elbarouni, A. Budaj, K. A. A. Fox, J. M. Gore, D. Brieger, J. López-Sendón, A. Langer, F. van de Werf, P. G. Steg, and A. T. Yan, "Comparative prognostic value of T-wave inversion and ST-segment depression on the admission electrocardiogram in non–ST-segment elevation acute coronary syndromes," *Amer. Heart J.*, vol. 166, no. 2, pp. 290–297, Aug. 2013, doi: 10.1016/j.ahj.2013.04.010.

[8] C.-K. Wong, W. Gao, R. A. Stewart, J. K. French, P. E. Aylward, J. Benatar, and H. D. White, "Prognostic value of lead v 1 ST elevation during acute inferior myocardial infarction," *Circulation*, vol. 122, no. 5, pp. 463–469, Aug. 2010, doi: 10.1161/CIRCULATIONAHA.109.924068.

[9] A. G. Kleber, "ST-segment elevation in the electrocardiogram: A sign of myocardial ischemia," *Cardiovascular Res.*, vol. 45, no. 1, pp. 111–118, Jan. 2000, doi: 10.1016/s0008-6363(99)00301-6.

[10] J. E. Deanfield, "Transient ST-segment depression as a marker of myocardial ischemia during daily life," *Amer. J. Cardiol.*, vol. 54, no. 10, pp. 1195–1200, Dec. 1984, doi: 10.1016/S0002-9149(84)80066-1.

[11] I. J. Nañez-Gil, H. Riha, and H. Ramakrishna, "Review of the 2017 European society of Cardiology's guidelines for the management of acute myocardial infarction in patients presenting with ST-segment elevation and focused update on dual antiplatelet therapy in coronary artery disease developed in collaboration with the European association for cardiothoracic surgery," *J. Cardiothoracic Vascular Anesthesia*, vol. 33, no. 8, pp. 2334–2343, Aug. 2019, doi: 10.1053/j.jvca.2018.09.032.

[12] M. H. Crawford, R. A. O'Rourke, and F. L. Grover, "Mechanism of inferior electrocardiographic ST-segment depression during acute anterior myocardial infarction in a baboon model," *Amer. J. Cardiol.*, vol. 54, no. 8, pp. 1114–1117, Nov. 1984, doi: 10.1016/s0002-9149(84)80155-1.

[13] B. Hopenfeld, J. G. Stinstra, and R. S. Macleod, "Mechanism for ST depression associated with contiguous subendocardial ischemia," *J. Cardiovascular Electrophysiol.*, vol. 15, no. 10, pp. 1200–1206, Oct. 2004, doi: 10.1046/j.1540-8167.2004.04072.x.

[14] S. Figliozzi, A. Stazi, G. Pinnacchio, M. Laurito, R. Parrinello, A. Villano, G. Russo, M. Milo, R. Mollo, G. A. Lanza, and F. Crea, "Use of T-wave alternans in identifying patients with coronary artery disease," *J. Cardiovascular Med.*, vol. 17, no. 1, pp. 20–25, Jan. 2016, doi: 10.2459/JCM.0000000000000080.

[15] C. Van Mieghem, M. Sabbe, and D. Knockaert, "The clinical value of the ECG in noncardiac conditions," *Chest*, vol. 125, no. 4, pp. 1561–1576, Apr. 2004, doi: 10.1378/chest.125.4.1561.

[16] U. R. Acharya, H. Fujita, M. Adam, O. S. Lih, V. K. Sudarshan, T. J. Hong, J. E. Koh, Y. Hagiwara, C. K. Chua, C. K. Poo, and T. R. San, "Automated characterization and classification of coronary artery disease and myocardial infarction by decomposition of ECG signals: A comparative study," *Inf. Sci.*, vol. 377, pp. 17–29, Jan. 2017, doi: 10.1016/j.ins.2016.10.013.

[17] U. R. Acharya, O. Faust, V. Sree, G. Swapna, R. J. Martis, N. A. Kadri, and J. S. Suri, "Linear and nonlinear analysis of normal and CAD-affected heart rate signals," *Comput. Methods Programs Biomed.*, vol. 113, no. 1, pp. 55–68, Jan. 2014, doi: 10.1016/j.cmpb.2013.08.017.

[18] Q. U. Mastoi, T. Y. Wah, R. Gopal Raj, and U. Iqbal, "Automated diagnosis of coronary artery disease: A review and workflow," *Cardiology Res. Pract.*, vol. 2018, Feb. 2018, Art. no. 2016282, doi: 10.1155/2018/2016282.

[19] R. Alizadehsani, M. J. Hosseini, A. Khosravi, F. Khozeimeh, M. Roshanzamir, N. Sarrafzadegan, and S. Nahavandi, "Non-invasive detection of coronary artery disease in high-risk patients based on the stenosis prediction of separate coronary arteries," *Comput. Methods Prog. Biomed.*, vol. 162, pp. 119–127, Aug. 2018, doi: 10.1016/j.cmpb.2018.05.009.

[20] U. R. Acharya, V. K. Sudarshan, J. E. W. Koh, R. J. Martis, J. H. Tan, S. L. Oh, A. Muhammad, Y. Hagiwara, M. R. K. Mookiah, K. P. Chua, C. K. Chua, and R. S. Tan, "Application of higher-order spectra for the characterization of coronary artery disease using electrocardiogram signals," *Biomed. Signal Process. Control*, vol. 31, pp. 31–43, Jan. 2017, doi: 10.1016/j.bspc.2016.07.003.

[21] S. Patidar, R. B. Pachori, and U. R. Acharya, "Automated diagnosis of coronary artery disease using tunable-Q wavelet transform applied on heart rate signals," *Knowl.-Based Syst.*, vol. 82, pp. 1–10, Jul. 2015, doi: 10.1016/j.knosys.2015.02.011.

[22] M. Kumar, R. B. Pachori, and U. R. Acharya, "An efficient automated technique for CAD diagnosis using flexible analytic wavelet transform and entropy features extracted from HRV signals," *Expert Syst. Appl.*, vol. 63, pp. 165–172, Nov. 2016, doi: 10.1016/j.eswa.2016.06.038.

[23] D. Giri, U. R. Acharya, R. J. Martis, S. V. Sree, T.-C. Lim, T. Ahamed, and J. S. Suri, "Automated diagnosis of coronary artery disease affected patients using LDA, PCA, ICA and discrete wavelet transform," *Knowl.-Based Syst.*, vol. 37, pp. 274–282, Jan. 2013, doi: 10.1016/j.knosys.2012.08.011.

[24] W. S. Kim, S. H. Jin, Y. K. Park, and H. M. Choi, "A study on development of multi-parametric measure of heart rate variability diagnosing cardiovascular disease," in *Proc. World Congr. Med. Physics Biomed. Eng.*, Seoul, South Korea, Aug./Sep. 2007, pp. 3480–3483.

[25] A. Kaveh and W. Chung, "Automated classification of coronary atherosclerosis using single lead ECG," in *Proc. IEEE Conf. Wireless Sensor (ICWISE)*, Kuching, Malaysia, Dec. 2013, pp. 108–113.

[26] H. G. Lee, K. Y. Noh, and K. H. Ryu, "Mining biosignal data: Coronary artery disease diagnosis using linear and nonlinear features of HRV," in *Proc. Pacific–Asia Conf. Knowl. Discovery Data Mining*, Nanjing, China, May 2007, pp. 218–228.

[27] H. G. Lee, K. Y. Noh, and K. H. Ryu, "A data mining approach for coronary heart disease prediction using HRV features and carotid arterial wall thickness," in *Proc. Int. Conf. Biomed. Eng. Informat.*, Sanya, China, May 2008, pp. 200–206.

[28] G. Piccirillo, D. Magri, S. Matera, M. Magnanti, A. Torrini, E. Pasquazzi, E. Schifano, S. Velitti, V. Marigliano, R. Quaglione, and F. Barilla, "QT variability strongly predicts sudden cardiac death in asymptomatic subjects with mild or moderate left ventricular systolic dysfunction: A prospective study," *Eur. Heart J.*, vol. 28, no. 11, pp. 1344–1350, Jun. 2007, doi: 10.1093/eurheartj/ehl367.

[29] P. Oosterhoff, L. G. Tereshchenko, M. A. G. van der Heyden, R. N. Ghanem, B. J. Fetics, R. D. Berger, and M. A. Vos, "Short-term variability of repolarization predicts ventricular tachycardia and sudden cardiac death in patients with structural heart disease: A comparison with QT variability index," *Heart Rhythm*, vol. 8, no. 10, pp. 1584–1590, Oct. 2011, doi: 10.1016/j.hrthm.2011.04.033.

[30] M. N. Niemeijer, M. E. van den Berg, M. Eijgelsheim, G. van Herpen, B. H. Stricker, J. A. Kors, and P. R. Rijnbeek, "Short-term QT variability markers for the prediction of ventricular arrhythmias and sudden cardiac death: A systematic review," *Heart*, vol. 100, no. 23, pp. 1831–1836, Dec. 2014, doi: 10.1136/heartjnl-2014-305671.

[31] M. Baumert, A. Porta, M. A. Vos, M. Malik, J.-P. Couderc, P. Laguna, G. Piccirillo, G. L. Smith, L. G. Tereshchenko, and P. G. A. Volders, "QT interval variability in body surface ECG: Measurement, physiological basis, and clinical value: Position statement and consensus guidance endorsed by the European heart rhythm association jointly with the ESC working group on cardiac cellular electrophysiology," *Europace*, vol. 18, no. 6, pp. 925–944, Jun. 2016, doi: 10.1093/europace/euv405.

[32] Y. Li, P. Li, C. Karmakar, and C. Liu, "Distribution entropy for short-term QT interval variability analysis: A comparison between the heart failure and normal control groups," in *Proc. Comput. Cardiol. Conf. (CinC)*, Hangzhou, China, Sep. 2015, pp. 309–312.

[33] C. P. Dobson, M. T. La Rovere, C. Olsen, M. Berardinangeli, M. Veniani, P. Midi, L. Tavazzi, and M. Haigney, "24-hour QT variability in heart failure," *J. Electrocardiol.*, vol. 42, no. 6, pp. 500–504, Nov. 2009, doi: 10.1016/j.jelectrocard.2009.06.021.

[34] S. Nayyar, K. C. Roberts-Thomson, M. A. Hasan, T. Sullivan, J. Harrington, P. Sanders, and M. Baumert, "Autonomic modulation of repolarization instability in patients with heart failure prone to ventricular tachycardia," *Amer. J. Physiol.-Heart Circulatory Physiol.*, vol. 305, no. 8, pp. 1181–1188, Oct. 2013, doi: 10.1152/ajpheart.00448.2013.

[35] B. Porter, M. J. Bishop, S. Claridge, J. Behar, B. J. Sieniewicz, J. Webb, J. Gould, M. O'Neill, C. A. Rinaldi, R. Razavi, J. S. Gill, and P. Taggart, "Autonomic modulation in patients with heart failure increases Beat-to-Beat variability of ventricular action potential duration," *Frontiers Physiol.*, vol. 8, p. 328, May 2017, doi: 10.3389/fphys.2017.00328.

[36] M. A. Hasan, D. Abbott, and M. Baumert, "Beat-to-beat QT interval variability and T-wave amplitude in patients with myocardial infarction," *Physiol. Meas.*, vol. 34, no. 9, pp. 1075–1083, Sep. 2013, doi: 10.1088/0967-3334/34/9/1075.

[37] E. Nahshoni, B. Strasberg, E. Adler, S. Imbar, J. Sulkes, and A. Weizman, "Complexity of the dynamic QT variability and RR variability in patients with acute anterior wall myocardial infarction," *J. Electrocardiol.*, vol. 37, no. 3, pp. 173–179, Jul. 2004, doi: 10.1016/j.jelectrocard.2004.04.008.

[38] K. Hiromoto, H. Shimizu, T. Mine, T. Masuyama, and M. Ohyanagi, "Correlation between Beat-to-Beat QT interval variability and impaired left ventricular function in patients with previous myocardial infarction," *Ann. Noninvasive Electrocardiol.*, vol. 11, no. 4, pp. 299–305, Oct. 2006, doi: 10.1111/j.1542-474X.2006.00121.x.

[39] B. Vrtovec, V. Starc, and R. Starc, "Beat-to-beat QT interval variability in coronary patients," *J. Electrocardiol.*, vol. 33, no. 2, pp. 119–125, Apr. 2000, doi: 10.1016/s0022-0736(00)80068-0.

[40] T. Murabayashi, B. Fetics, D. Kass, E. Nevo, B. Gramatikov, and R. D. Berger, "Beat-to-beat QT interval variability associated with acute myocardial ischemia," *J. Electrocardiol.*, vol. 35, no. 1, pp. 19–25, Jan. 2002, doi: 10.1054/jelc.2002.30250.

[41] L. S. Liu, "Chinese guidelines for the management of hypertension," *Chin. J. Cardiol.*, vol. 39, no. 7, pp. 579–615, Jul. 2010.

[42] J. Weng, "Standards of care for type 2 diabetes in China," *Diabetes/Metabolism Res. Rev.*, vol. 32, no. 5, pp. 442–458, Jul. 2016, doi: 10.1002/dmrr.2827.

[43] I. Adults, "Chinese guideline for the management of dyslipidemia in adults," *Zhonghua Xin Xue Guan Bing Za Zhi*, vol. 44, no. 10, pp. 833–853, Oct. 2016, doi: 10.3760/cma.j.issn.0253-3758.2016.10.005.

[44] M. P. Judkins, "Percutaneous transfemoral selective coronary arteriography," *Radiologic Clinics North Amer.*, vol. 6, no. 3, pp. 467–492, Dec. 1968, doi: 10.1148/114.3.732.

[45] L. Yao, P. Li, C. Liu, Y. Hou, C. Yan, L. Li, K. Li, X. Wang, A. Deogire, C. Du, H. Zhang, J. Wang, and H. Li, "Comparison of QT interval variability of coronary patients without myocardial infarction with that of patients with old myocardial infarction," *Comput. Biol. Med.*, vol. 113, Oct. 2019, Art. no. 103396, doi: 10.1016/j.compbiomed.2019.103396.

[46] C. Vidaurre, T. H. Sander, and A. Schlogl, "BioSig: The free and open source software library for biomedical signal processing," *Comput. Intell. Neurosci.*, vol. 2011, Mar. 2011, Art. no. 935364, doi: 10.1155/2011/935364.

[47] V. X. Afonso, W. J. Tompkins, T. Q. Nguyen, and S. Luo, "ECG beat detection using filter banks," *IEEE Trans. Biomed. Eng.*, vol. 46, no. 2, pp. 192–202, Feb. 1999, doi: 10.1109/10.740882.

[48] X. Hu, J. Liu, J. Wang, Z. Xiao, and J. Yao, "Automatic detection of onset and offset of QRS complexes independent of isoelectric segments," *Measurement*, vol. 51, pp. 53–62, May 2014, doi: 10.1016/j.measurement.2014.01.011.

[49] Q. Zhang, A. I. Manriquez, C. Medigue, Y. Papelier, and M. Sorine, "An algorithm for robust and efficient location of T-Wave ends in electrocardiograms," *IEEE Trans. Biomed. Eng.*, vol. 53, no. 12, pp. 2544–2552, Dec. 2006, doi: 10.1109/TBME.2006.884644.

[50] M. P. Tarvainen, P. O. Ranta-aho, and P. A. Karjalainen, "An advanced detrending method with application to HRV analysis," *IEEE Trans. Biomed. Eng.*, vol. 49, no. 2, pp. 172–175, Feb. 2002, doi: 10.1109/10.979357.

[51] J. J. Goldberger, M. W. Ahmed, M. A. Parker, and A. H. Kadish, "Dissociation of heart rate variability from parasympathetic tone," *Amer. J. Physiol.-Heart Circulatory Physiol.*, vol. 266, no. 5, pp. H2152–H2157, May 1994, doi: 10.1152/ajpheart.1994.266.5.H2152.

[52] T. F. O. T. E. S. Electrophysiology, "Heart rate variability: Standards of measurement, physiological interpretation, and clinical use," *Circulation*, vol. 93, no. 5, pp. 1043–1065, Mar. 1996, doi: 10.1161/01.CIR.93.5.1043.

[53] M. Brennan, M. Palaniswami, and P. Kamen, "Do existing measures of poincare plot geometry reflect nonlinear features of heart rate variability?" *IEEE Trans. Biomed. Eng.*, vol. 48, no. 11, pp. 1342–1347, Nov. 2001, doi: 10.1109/10.959330.

[54] C. Yan, P. Li, L. Ji, L. Yao, C. Karmakar, and C. Liu, "Area asymmetry of heart rate variability signal," *Biomed. Eng. OnLine*, vol. 16, no. 1, p. 112, Sep. 2017, doi: 10.1186/s12938-017-0402-3.

[55] X. Wang, C. Yan, B. Shi, C. Liu, C. Karmakar, and P. Li, "Does the temporal asymmetry of short-term heart rate variability change during regular walking? A pilot study of healthy young subjects," *Computional Math. Methods Med.*, vol. 2018, p. 3543048, Apr. 2018, doi: 10.1155/2018/3543048.

[56] P. Li, C. Liu, K. Li, D. Zheng, C. Liu, and Y. Hou, "Assessing the complexity of short-term heartbeat interval series by distribution entropy," *Med. Biol. Eng. Comput.*, vol. 53, no. 1, pp. 77–87, Jan. 2015, doi: 10.1007/s11517-014-1216-0.

[57] I. W. Selesnick, "Wavelet transform with tunable Q-Factor," *IEEE Trans. Signal Process.*, vol. 59, no. 8, pp. 3560–3575, Aug. 2011, doi: 10.1109/TSP.2011.2143711.

[58] I. Bayram and I. W. Selesnick, "Frequency-domain design of overcomplete rational-dilation wavelet transforms," *IEEE Trans. Signal Process.*, vol. 57, no. 8, pp. 2957–2972, Aug. 2009, doi: 10.1109/TSP.2009.2020756.

[59] G. Altan, Y. Kutlu, and N. Allahverdi, "A new approach to early diagnosis of congestive heart failure disease by using Hilbert–Huang transform," *Comput. Methods Programs Biomed.*, vol. 137, pp. 23–34, Dec. 2016, doi: 10.1016/j.cmpb.2016.09.003.

[60] M. M. Saritas, "Performance analysis of ANN and naive Bayes classification algorithm for data classification," *Int. J. Intell. Syst. Appl. Eng.*, vol. 7, no. 2, pp. 88–91, Jan. 2019, doi: 10.18201/ijisae.2019252786.

[61] W. S. Noble, "What is a support vector machine?" *Nature Biotechnol.*, vol. 24, no. 12, pp. 1565–1567, Dec. 2006, doi: 10.1038/nbt1206-1565.

[62] T. Chen and C. Guestrin, "XGBoost: A scalable tree boosting system," in *Proc. 22nd ACM SIGKDD Int. Conf. Knowl. Discovery Data Mining*, San Francisco, CA, USA, Aug. 2016, pp. 785–794.

[63] K. He, X. Zhang, S. Ren, and J. Sun, "Deep residual learning for image recognition," in *Proc. IEEE Conf. Comput. Vis. Pattern Recognit. (CVPR)*, Las Vegas, NV, USA, Jun. 2016, pp. 770–778.

[64] F. Sahli Costabal, K. Matsuno, J. Yao, P. Perdikaris, and E. Kuhl, "Machine learning in drug development: Characterizing the effect of 30 drugs on the QT interval using Gaussian process regression, sensitivity analysis, and uncertainty quantification," *Comput. Methods Appl. Mech. Eng.*, vol. 348, pp. 313–333, May 2019, doi: 10.1016/j.cma.2019.01.033.

[65] L. Qu, V. L. Vetter, G. L. Bird, H. Qiu, and P. S. White, "A Na×00EF;ve Bayes classifier for differential diagnosis of long QT syndrome in children," in *Proc. IEEE Int. Conf. Bioinf. Biomed. (BIBM)*, Hong Kong, Dec. 2010, pp. 433–437.

[66] B. Li, J. L. Mendenhall, B. M. Kroncke, K. C. Taylor, H. Huang, D. K. Smith, C. G. Vanoye, J. D. Blume, A. L. George, C. R. Sanders, and J. Meiler, "Predicting the functional impact of KCNQ1 variants of unknown significance," *Circulation, Cardiovascular Genet.*, vol. 10, no. 5, Oct. 2017, doi: 10.1161/CIRCGENETICS.117.001754.

[67] R. D. Berger, "QT interval variability," *J. Amer. College Cardiology*, vol. 54, no. 9, pp. 851–852, Aug. 2009, doi: 10.1016/j.jacc.2009.06.007.

[68] G. Coppola, P. Caritá, E. Corrado, A. Borrelli, A. Rotolo, M. Guglielmo, C. Nugara, L. Ajello, M. Santomauro, and S. Novo, "ST segment elevations: Always a marker of acute myocardial infarction?" *Indian Heart J.*, vol. 65, no. 4, pp. 412–423, Jul. 2013, doi: 10.1016/j.ihj.2013.06.013.

[69] D. P. Kingma and J. Ba, "Adam: A method for stochastic optimization," 2014, *arXiv:1412.6980*. [Online]. Available: http://arxiv.org/abs/1412.6980

LIANKE YAO (Student Member, IEEE) received the B.S. degree in biomedical engineering from the Chongqing University of Technology, Chongqing, China, in 2012. He is currently pursuing the Ph.D. degree with Shandong University.

His research interests include biomedical signal processing, QT interval variability analysis, automated detection of arrhythmias, remote ECG monitoring, and machine learning.

CHANGCHUN LIU received the B.S. and M.S. degrees in automation from Shandong Industrial University (now merged into Shandong University), Jinan, China, in 1982 and 1987, respectively. Since 2000, he has been a Professor in biomedical engineering with the School of Control Science and Engineering, Shandong University, where he was the Head of the research group of Noninvasive Evaluation of Cardiovascular Function. He has authored over 100 articles, and he also holds more than 15 Chinese invention patents. His research interests include novel solutions for noninvasive detection of cardiovascular function, biomedical measurements, and biomedical devices.

Dr. Liu was a recipient of the First Prize of the Science and Technology Award in technical invention awarded by the Ministry of Education, China, in 2003, and the Second Prize of the Science and Technology Award in invention awarded by Shandong Province, China, in 2016.

PENG LI (Member, IEEE) received the B.S. and Ph.D. degrees in biomedical engineering from Shandong University, Jinan, China, in 2009 and 2014, respectively.

He has obtained multiple disciplinary postdoctoral trainings first at Shandong University from 2014 to 2015 and then at Harvard Medical School from 2016 to 2018. He is currently appointed as an Instructor in Medicine with the Division of Sleep Medicine, Harvard Medical School, Boston, MA, and an Associate Physiologist with the Division of Sleep and Circadian Disorders, Brigham and Women's Hospital (BWH), Boston. He is codirecting a cross-disciplinary training program at the BWH, namely, Medical Biodynamics Program. His research focuses on understanding nonlinear dynamics in the cardiovascular system, brain activity, and motor activity, and their relationship with health. In particular, he is interested in noninvasively at preclinical stages identifying individuals with an increased risk of Alzheimer's disease and cardiovascular diseases. In addition, he also focused recently on the comprehensive assessment of cancer prognosis with physiological monitoring.

Dr. Li is a member of the Society for Neuroscience, Sleep Research Society, American Academy of Sleep Medicine, China Biomedical Engineering Society, and Beijing Society for Cognitive Neuroscience. He was a recipient of the Trainee Professional Development Award from the Society for Neuroscience, in 2018, and a recipient of the Second Prize of the Science and Technology Award in invention awarded by Shandong Province, China, in 2016.

JIKUO WANG received the B.S. degree in electrical engineering and its automation and the M.S. degree in control science and engineering from Qufu Normal University, China, in 2012 and 2015, respectively. He is currently pursuing the Ph.D. degree in biomedical engineering with Shandong University.

His current research interests include deep learning and medical image analysis.

YUANYUAN LIU received the Ph.D. degree in biomedical engineering from Shandong University, Jinan, China, in 2014.

Since 2008, she has been a Lecturer in biomedical engineering with the School of Control Science and Engineering, Shandong University. Her research interests include biomedical signal processing, altitude acclimatization modeling, the sleep signal analysis, and Chinese medicine.

WANG LI received the bachelor's degree from the Harbin Institute of Technology, in 2009. He participated a successive postgraduate and doctoral programs of study in Chongqing University from 2011 to 2016, where he majored in biomedical engineering.

He currently works at the Chongqing University of Technology. His research interests include noninvasive disease detection technology and device, and e-nose systems for disease detection.

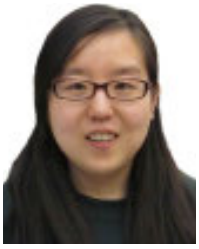

XINPEI WANG received the B.S. and Ph.D. degrees in biomedical engineering from Shandong University, Jinan, China, in 2005 and 2011, respectively. She is currently a Lecturer with the School of Control Science and Engineering, Shandong University.

Her current research interests include biomedical signal and image processing, machine learning, and biomedical measurements and devices.

HAN LI received the B.S. degree in automation from Shandong University, Jinan, China, in 2014. She is currently pursuing the Ph.D. degree with the School of Control Science and Engineering, Shandong University.

Her current research interests include the application of computational intelligence in the detection of cardiovascular diseases and biomedical signal processing.

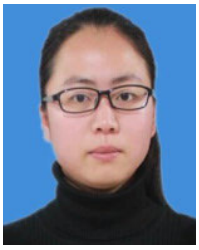

HUAN ZHANG received the B.S. degree in electronic science and technology from Shanxi University, Taiyuan, China, in 2013. She is pursuing the Ph.D. degree with the School of Control Science and Engineering, Shandong University, China.

Her research interests include biomedical signal processing, machine learning, and early detection of coronary artery disease.